INDERSCIENCE PUBLISHERS
Linking academia, business and industry through research

International Journal of Computational Science and Engineering

ISSN online: 1742-7193 - ISSN print: 1742-7185
https://www.inderscience.com/ijcse

Research on mobile robot path planning and tracking control

Jieyun Yu

DOI: 10.1504/IJCSE.2023.10054169

Article History:

Received:	07 June 2022
Last revised:	01 October 2022
Accepted:	13 October 2022
Published online:	12 July 2023

Research on mobile robot path planning and tracking control

Jieyun Yu

School of Mathematics,
Jinan University,
Guangzhou, 510632, China
Email: 15919575526@163.com

Abstract: Autonomous navigation of a robot is a promising research domain due to its extensive applications in which planning and motion control are the most important and interesting parts. The proposed techniques are classified into two main categories: the first group focuses on the improvement of model free adaptive control (MFAC) to meet the extreme performances of the control system, and the second concentrates on the classic artificial potential field (APF) algorithm to deal with the limitations like falling into local minima and a non-reachable goal problem. This paper proposes a novel exponential feedforward-feedback control strategy based on iterative learning control (ILC) MFAC to the reference trajectory tracking, and then introduces a virtual target with exponential coordinated form to realise local risk collision avoidance for path planning. Compared to some traditional models, our proposed methods have a faster trajectory convergence rate, lower avoidable error, and higher safe performance. The simulation results verify that our work would bring meaningful insights to future intelligent navigation research.

Keywords: trajectory tracking; path planning; model-free adaptive control; artificial potential field; exponential-form virtual target.

Reference to this paper should be made as follows: Yu, J. (2023) 'Research on mobile robot path planning and tracking control', *Int. J. Computational Science and Engineering*, Vol. 26, No. 4, pp.349–360.

Biographical notes: Jieyun Yu received her Bachelor's degree from the Hanshan Normal University in 2019. Currently, she is pursuing her MS at the College of Mathematics, Jinan University, Guangzhou, China. Her research interests are related to robot path planning and system dynamic.

1 Introduction

Path planning and trajectory tracking are the core technologies in the decision-making and control of mobile robots. When an autonomous robot moves from a point to a target point in its given environment, it is essential to plan a collision free path in its way, and answer to some criterion of autonomy requirements, such as energy, time, and safety. Many debugging techniques are proposed by scholars, and related enterprises attached great significance to increase investment in security control field, but accidents still occur. The trend for automatic machines is to operate at higher speed, but it may hinder the accuracy and repeatability of the robot motion, since extreme performances are required from the control system. At the same time, the route should be harmless. Therefore, our framework mainly consists of two parts: IMFAC-based control strategy of trajectory tracking and IAPF-based path planning for obstacle avoidance.

Precision control is desirable in high performance robotics and automation systems. Many techniques, as well as proportional-integral-derivative (PID) (Patra and Mohapatra, 2022), optimisation algorithm, and neural network (Naik et al., 2012), have been utilised to deal with this problem. For example, Patra and Mohapatra (2022) presented the coordinated control of PI type PSS and MISO damping controller by using SSSC-based PI type lead lag controller for transient stability analysis. By considering the possible limitations of network communication, Wu and Liu (2019) proposed a networked predictive control algorithm based on model free adaptive control to compensate the delay caused by network. The MFAC has been used to reject the sensor noise measuring the control output to deal with control problems such as strongly nonlinear and time-varying systems. Its basic idea is to use a newly introduced concept of pseudo gradient vector or pseudo Jacobi matrix and pseudo order, using a series of dynamic linear time-varying models to replace the general discrete-time nonlinear system near the trajectory of the controlled system, and the pseudo gradient vector is estimated online with the I/O data of the controlled system to realise model-free adaptive control. Iterative learning control (ILC) is mainly aimed at repeatable systems in finite time, which is divided into open-loop ILC and closed-loop ILC (Noueili et al., 2017). The learning process of open-loop ILC may produce large errors and slow

convergence speed, while the closed-loop ILC needs high gain feedback, which may produce too large control signals and affect the convergence speed of the system. In Mateo and Sugimoto (2015), a feedback feedforward controller is designed to improve the control quality of the existing MFAC control system. However, the treatment of MFAC is still a matter of controversy. In this paper, the exponential adjustment factor is used to further modify the feedforward-feedback control law for improving the convergence speed of the system and reducing the error.

Classical path planning methods include artificial potential field method (Xueqiang, 2014), A^* algorithm (Song et al., 2019), dynamic window method (Eduardo et al., 2019), etc. Most of the approaches for path planning focus on minimising path length. However, the drawbacks associated with these approaches are as follows: it takes more computational time in large problem space and more likely to close to the obstacles. In this paper, we refer to the APF to develop a path planning algorithm. The artificial potential field method was proposed by Khatib, it is widely used in real-time obstacle avoidance and smooth trajectory control due to its simple principle, less calculation and fast processing speed, but the traditional artificial potential field method has the problems of target unreachable and local minimum. The potential field can be improved by using a mixture of potential and positioning risk fields that generates a hybrid directional flow to produce a safe and efficient path (Shin and Kim, 2021) or setting virtual targets to guide a robot out of the dead zone (Jinchao and Yu, 2013). The traditional artificial potential field method regards the obstacle as a particle, and the planned path may pass through the interior of the obstacle, what more, in the real environment, the shape of the obstacles themselves can not be ignored. If the external geometry of the obstacle is a concave polygon, it is difficult to get out of the area only by relying on the artificial potential field. Even if the ideal 'walk around the wall' strategy (Luo et al., 2011) is adopted, it will take a long time to produce a long path. If the number of the path turning points planned by the algorithm is too large, it will inevitably increase the difficulty of trajectory tracking control. Based on the existing improvement of repulsion field function (Xueqiang, 2014), this paper takes points from classical continuous obstacles such as U-type and L-type instead of the potential field when the obstacles are regarded as particles, and them sets temporary virtual targets according to the environmental judgment conditions in Zhao and Li (2017). The exponential factor is introduced to adjust the virtual target position to eliminate singular values, reduce the number of turns and enhance the path security.

Inspired by the background described above and using previous research conducted by the scholars for the obstacle avoidance and trajectory tracking cases based on APF and I-MFAC, this work presents an extension of the proposed method to solve the problem of collision avoidance. The contributions of this paper are mainly as follows:

1 Novel application of ICL-MFAC algorithm for power system controls which achieves high tracking precision, and the satisfied result indicates the good application of MFAC on industrial production.

2 Development of a virtual target point-based obstacle avoidance scheme. The designed local path planning method can adapt to a cluttered environment and apply to real delivery tasks in automotive assembly process.

3 The proposed control algorithms are easy to implement and reduces the amount of computation, which is beneficial for engineering popularisation.

The rest of this paper is organised as follows. Section 2 gives the basic principle of the dynamic characteristic of ICL-MFAC in brief, and presents the design procedure of the proposed exponential feedforward-feedback MFAC, then simulation experiments are given to illustrate the effectiveness of our scheme, Section 3 discusses the fundamental of APF for mobile robot path planning, then the reasons of the defects are analysed and the corresponding resolutions are established to modified the virtual sub-target position, then comparative simulation certificates are carry out. Section 4 analyses the limitations of the schemes. Section 5 concludes the paper.

2 Feedback-feedforward ILC system based on MFAC

2.1 System description

The nonlinear system with m-dimensional input and q-dimensional output is given as follows (Ren and Hou, 2020):

$$y_n(k+1) = f\left(u_n(k), y_n(k), \xi(k), (k)\right) \tag{2.1.1}$$

where $k \in \{0, 1, \ldots, K\}$, $k \in [0, K]$ is the time indicator, n is the number of iterations, $y_n(k)$ is the system output at time k of the n^{th} iteration, $u_n(k)$ is the corresponding control input, $\xi(k)$ is the repeated bounded external interference.

Suppose $f(u_n(k), y_n(k), \xi(k), k)$ satisfies the uniform global Lipschitz condition. If $y_d(k)$ is the preset desired trajectory, there exists a unique bounded control $u_d(k)$ such that:

$$y_d(k+1) = f\left(u_d(k), y_d(k), \xi(k), (k)\right) \tag{2.1.2}$$

A feedback-feedforward ILC system based on MFAC, where the feedback control term stabilises the system and the feedforward control term compensates for repeatable nonlinear time-varying dynamics and disturbances, enhances the control performance achieved through feedback alone (Ren and Hou, 2020). In order to accelerate convergence, we add parameters α to the control law as follows:

$$u_n(k) = u_n^f(k) + u_n^b(k) \tag{2.1.3}$$

$$u_n^f(k) = u_{n-1}^f(k) + \beta e_{n-1}(k+1) \tag{2.1.4}$$

$$u_n^b(k) = u_n^b(k-1) + \frac{\rho\hat{\phi}_n(k)}{\lambda + \alpha\left|\hat{\phi}_n(k)\right|^2} \times\left[y_d(k+1) - y_n(k)\right] \tag{2.1.5}$$

$$\hat{\phi}_n(k) = \hat{\phi}_n(k-1) + \frac{\eta\Delta u_n^b(k-1)}{\mu + \alpha\left|\Delta u_n^b(k-1)\right|^2} \times\left[\Delta y_n(k) - \hat{\phi}_n(k-1)\Delta u_n^b(k-1)\right] \tag{2.1.6}$$

$$\hat{\phi}_n(k) = \hat{\phi}_n(1), \text{ if } \hat{\phi}_n(k) \le \varepsilon \text{ or } \left|\Delta u_n^b(k-1)\right| \le \varepsilon.$$

where $e_n(k) = y_d(k) - y_n(k)$ denotes the tracking error of the nth iteration, u_n^f is feedforward part, and u_n^b is the feedback part. μ is the weighting factor that limits the variance of the control input, and η is the learning rate.

Theorem 1 (Ren and Hou, 2020): The system described by equation (2.1.1) under the action of control algorithm (2.1.3)~(2.1.6), if $\|I - \beta f_u(\varsigma_n)\| < 1$, then we have:

$$\lim_{n\to\infty}\left\|u_d(k) - u_n^f(k)\right\|_\lambda \le \sigma \tag{2.1.7}$$

$$\lim_{n\to\infty}\left\|y_d(k) - y_n(k)\right\| \le \sigma \tag{2.1.8}$$

where $\sigma > 0$ is an appropriate constant, when $\|e_n(0)\| = 0$ and $\left\|u_n^b(0)\right\| = 0$ are satisfied and $y_d(k)$ are constants, the feedback-feedforward ICL system based on MFAC is convergent, that is, the following equations holds:

$$\lim_{n\to\infty}\left\|u_d(k) - u_n^f(k)\right\|_\lambda = 0 \tag{2.1.9}$$

$$\lim_{n\to\infty}\left\|y_d(k) - y_n(k)\right\| = 0 \tag{2.1.10}$$

2.2 Modified feedforward-feedback control law

Since the system (2.1.1) is unknown, in a sequel, the system time-varying parameter in equations (2.1.3)~(2.1.6) is also unknown. To make the control system designing simple and easy to be used in practice, the exponential terms are introduced to replace the squared term $\left|\Delta u_n^b(k-1)\right|^2$ and $\left|\hat{\phi}_n(k)\right|^2$ to modify the feedforward-feedback model-free adaptive control law as follows:

$$u_n^b(k) = u_n^b(k-1) + \frac{\rho\cdot\hat{\phi}_n(k)}{\lambda + \alpha e^{-\arctan\left(\pi\left|\hat{\phi}_n(k)\right|\right)}} \times\left[y_d(k+1) - y_n(k)\right] \tag{2.2.1}$$

$$\hat{\phi}_n(k) = \hat{\phi}_n(k-1) + \frac{\eta\Delta u_n^b(k-1)}{\mu + \alpha e^{-\arctan\left(\pi\left|\Delta u_n^b(k-1)\right|\right)}} \times\left[\Delta y_n(k) - \hat{\phi}_n(k-1)\Delta u_n^b(k-1)\right] \tag{2.2.2}$$

2.3 Simulation experiment

The initial values of the dynamic system are set as follows: $\eta = 1$, $\rho = 0.2$, $\lambda = 1$, $\mu = 2$, $\theta = 2$, and the iterative learning gain $\beta = 0.4$. In order to show the effectiveness of the modified MFAC. Two control algorithms: the proposed I-MFAC (2.2.1), (2.2.2) and the conventional I-MFAC case (Ren and Hou, 2020) are for the comparison with the same initial parameters. Consider the following nonlinear discrete system which is parametrically time-varying and structurally time-varying:

$$y(k+1) = \begin{cases} \dfrac{y(k)u(k)}{1+y(k)^2} + \left[u(k) + a(k)\sin\left(y(k)\right)\right]^3, & k < 250 \\ \dfrac{y(k)u(k)}{1+y(k)^2} + u(k)^3, & 250 \le k \le 500 \end{cases}$$

$$y_d(k+1) = \begin{cases} 0.5(-1)^{round\left(\frac{k}{100}\right)}, & k < 250 \\ 0.5\sin\left(\dfrac{k\pi}{100}\right) + 0.3\cos\left(\dfrac{k\pi}{50}\right), & 250 \le k \le 500 \end{cases}$$

The experiment result is shown in Figures 2 and 3.

Figure 1 The block diagram of proposed feedback model-free adaptive control law

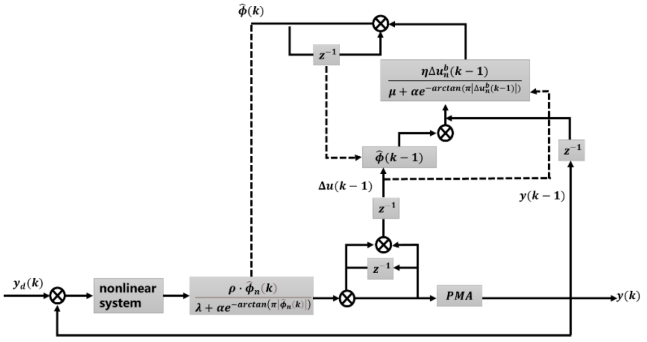

From Figures 2(a) and 3, it is obvious that although the control accuracy of conventional MFAC+ILC is good, the performance of tracking curve is not very ideal and prone to jitter, and the execution of a reference tracking performance by using our proposed scheme is superior when the value of α is equal or less than 1. As shown in Figure 2(b) and Table 1, the tracking effect of the proposed I-MFAILC algorithm is already the best when the number of iterations reaches 15, the tracking error plot shows that the tracking error of the exponential improved IMFAC is smaller than that of the conventional MFAC + ILC algorithm. What more, the time cost is reduced about 54.55%, which displays the superiority of our method.

Table 1 Performance indices for the number of *n*-iteration

Iteration/nth		*10*	*15*	*55*	*85*	*Convergent time/s*
MSE	Conventional IMFAC	0.025	0.015	0.008	0.003	1.5
	Our method	0.005	7.999 × 10^{-9}	0.004	1.637 × 10^{-7}	3.3

Figure 2 The adaptability performance comparison of conventional IMFAC and our method ($\alpha = 1$), (a) trajectory tracking (b) tracking mean squared error (see online version for colours)

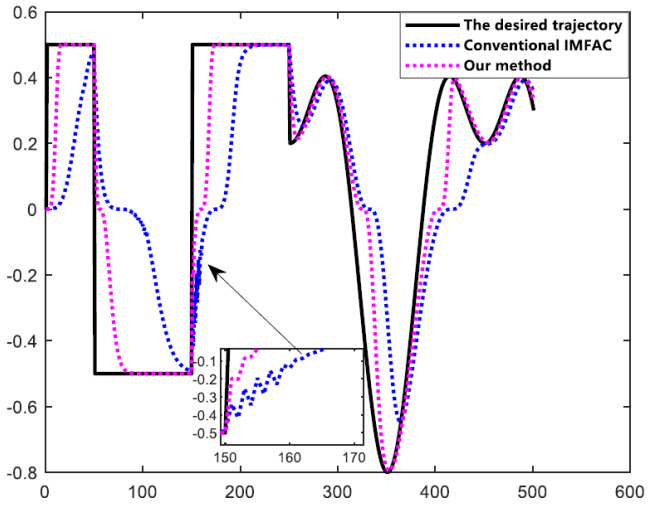

(a)

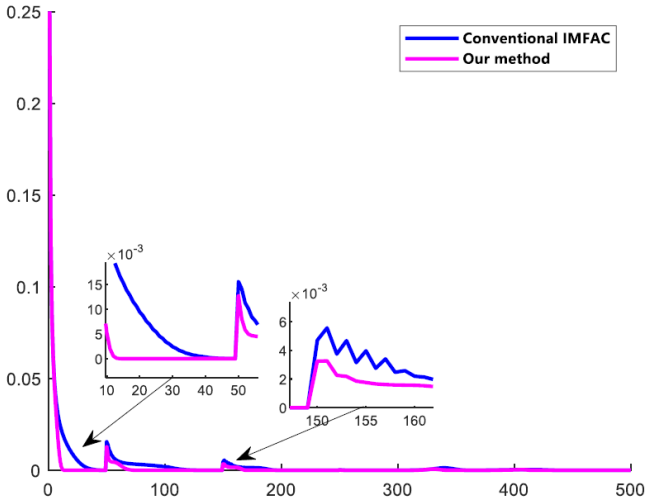

(b)

Figure 3 Comparative trajectory tracking at several values of α (see online version for colours)

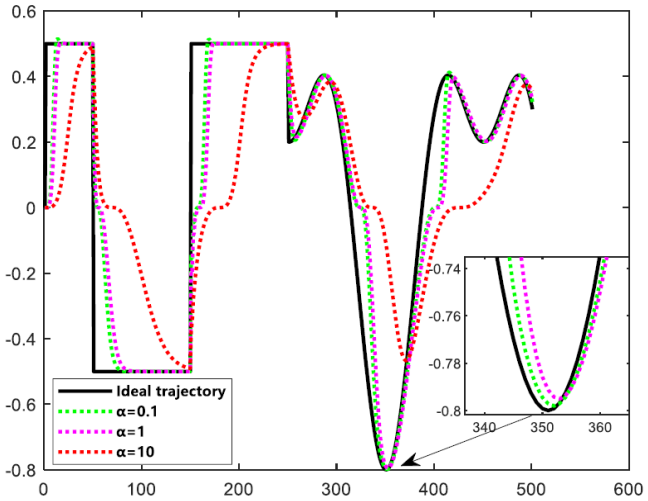

3 The APF method

3.1 Traditional APF model

In the areas of advanced robotics, the desired trajectory is determined at first and the dynamic system of the robot is controlled so that it will follow the desired trajectory exactly at every time step. However, an autonomous mobile robot (AMR) also needs to overcome many other challenges to become autonomous. One of the difficulties is to have efficient sensing system capable of determining routes while avoiding obstacles and building or updating its environment map. In this section, the framework of the local motion planning to realise obstacle avoidance is designed by utilising potential field. The workspace Q is comprehended as an environment of two dimensions or three dimensions, which contains several obstacles $O_j = [O_0, O_1, \ldots, O_m]$, where m denotes the number of obstacles. The mobile robot configuration is denoted by $X = (x, y, \theta)$ or $X = (x, y, z, \theta, \psi)$. Here we just talk about the situation of two dimensions. The Cartesian coordinates x and y represent the centre point of the mobile robot. The term θ denotes the orientation, i.e., θ indicates the angular difference between the environment and the mobile robot reference frame. The primary path planning objective is to generate a viable sequence of positions $Q_G = [X_0, X_1, \ldots, X_f]$ to drive the mobile robot safely from a given start position to a target position.

The robot is presented as a particle under the effect of an artificial potential field, whose local variation returns the free space structure. The main idea of the artificial potential field method is to build an attractive potential field around the goal, as well as to create a repulsive potential field force around the obstacles. Therefore, the artificial potential field method employs attractive and repulsive components to drive the mobile robot to its target while avoiding collisions with the obstacles. The total artificial potential field denoted by $U(X)$ and described by equation (3.1.1) is composed by two potential functions, the attractive potential $U_{att}(X)$, and the repulsive potential $U_{rep}(X)$. Therefore, the artificial potential field $U(X)$ is the superposition of these two functions as follows:

$$U(X) = U_{att}(X) + \sum_{i=1}^{n} U_{rep}(X) \tag{3.1.1}$$

Assuming that the robot position denotes X and the global target position denotes X_g, the gravitational potential field function is described by:

$$U_{att} = 0.5\,\kappa\rho^2(X, X_g) \tag{3.1.2}$$

where κ is the gravitational field gain coefficient. Gravity is a negative gradient of gravitational potential field:

$$F_{att} = -grad(U_{att}) = -\kappa\rho(X, X_g) \tag{3.1.3}$$

It is not difficult to see that the magnitude of gravity is directly proportional to the distance between the robot and the target point. The further the distance, the greater the gravity. The repulsive potential field function is described by:

$$\begin{cases} U_{rep}(X) = 0.5\,\beta\left(\dfrac{1}{\rho}-\dfrac{1}{P_o}\right)^2, & \rho \le P_o \\ U_{rep}(X) = 0, & \rho > P_o \end{cases} \tag{3.1.4}$$

where β denotes the repulsion field gain coefficient, P_o is the influence radius of the obstacle, and ρ denotes the distance between the robot and the obstacle. The repulsion force is a negative gradient of repulsion field function:

$$\begin{cases} F_{rep}(X) = \beta\left(\dfrac{1}{\rho}-\dfrac{1}{P_o}\right)\dfrac{1}{\rho^2}\dfrac{\partial\rho}{\partial X}, & \rho \le P_o \\ F_{rep}(X) = 0, & \rho > P_o \end{cases} \tag{3.1.5}$$

The superposition of repulsion and gravity is the resultant force:

$$F(X) = F_{att}(X) + \sum_{i=1}^{n} F_{rep}(X) \tag{3.1.6}$$

Figure 4 Moving direction of robot in APF

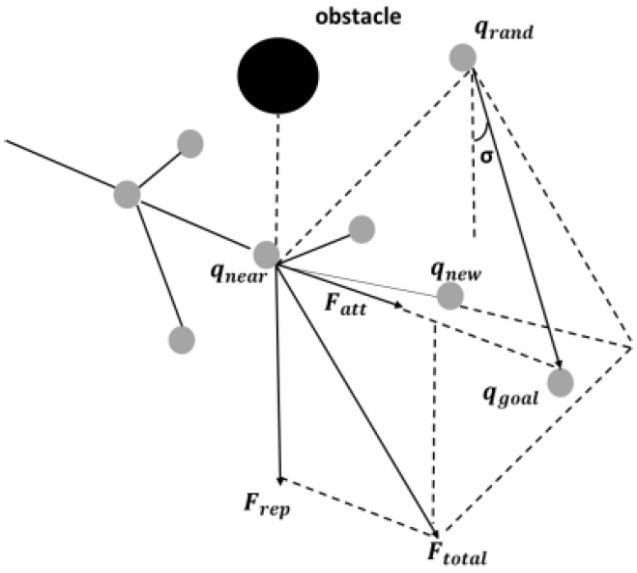

3.2 Shortcomings of the traditional APF

Although the traditional APF is one of the most representative in local path planning methods, there are still some defects. On one hand, if the goal is within the effective scope of the obstacles, a mobile robot would fail to reach the target position, which is called goal non-reachable with obstacle nearby (GNRON). GNRON problem arises while the goal is within the influence distance of the obstacle, which makes the global minimum of the total potential field is not at the goal position. This situation is due to the fact that as the robot approaches the goal, on one hand the attractive potential decreases, on the other hand the repulsive potential increases quickly. One of the ways to solve such puzzles is to do some optimisations of the repulsive potential field to balance the changes of two kind of force, especially the rapid increase of the repulsive force. It is found that if the repulsive potential approaches zero as a robot approaches the target, the total potential will take the global minimum at the goal. This motivates us to construct a new repulsive potential function which takes the relative distance between the robot and the goal into consideration as follows:

$$\begin{cases} F_{att} = -\kappa\left(X - X_g\right), & \rho\left(X, X_g\right) \le d \\ F_{att} = \dfrac{-d\kappa\left(X - X_g\right)}{\rho\left(X, X_g\right)}, & \rho\left(X, X_g\right) > d \end{cases} \tag{3.2.1}$$

where d is the action distance threshold of the global target point.

On the other hand, to handle with the problem of target unreachable caused by local minima, Zhao and Li (2017) added the influence of the distance between robot and target point to the repulsion field function of traditional artificial potential field method, so that the potential field at the target point is the global minimum point, and the repulsion potential field function by adding the distance is defined as follows:

$$U_{rep} = 0.5\,\beta\left(\frac{1}{\rho}-\frac{1}{P_o}\right)^2\left(X - X_g\right)^n,\ \rho \le P_o \tag{3.2.2}$$

The corresponding repulsion function can be expressed as:

$$\begin{aligned} F_{rep} = {} & \beta\left(\frac{1}{\rho}-\frac{1}{P_o}\right)\frac{1}{\rho^2}\frac{\partial\rho}{\partial X}\left(X - X_g\right)^n \\ & +0.5\,n\beta\left(\frac{1}{\rho}-\frac{1}{P_o}\right)^2\left(X - X_g\right)^{n-1} \end{aligned} \tag{3.2.3}$$

3.3 Conditions for judging local minimum

Zhao and Li (2017) analysed such a problem and put forward to the conditions for judging the robot entering the local minimum region when the following two Inequalities are meet:

$$\begin{cases} \left|\dfrac{F_{att} - F_{rep}}{F_{att}}\right| < \varepsilon \\ -1 \le \cos\left(\angle F_{att} - \angle F_{rep}\right) \le 0 \end{cases} \tag{3.3.1}$$

We employ the following judgment conditions according to Zhao and Li (2017) to carry out simulation experiments:

$$\begin{cases} \left|\dfrac{F_{att} - F_{rep}}{F_{att}}\right| < 0.5 \\ \cos\left(\angle F_{att} - \angle F_{rep}\right) \le -0.9 \end{cases} \tag{3.3.2}$$

when the robot is in or about to be in the equilibrium state, the motion direction is perpendicular to the gravity plane and a temporary virtual target would be set to guide the robot out of the trap, after that, the virtual target would be removed and the real target point leads the robot to continue moving to the destination. The coordinates of temporary virtual targets $\overline{G}$ under the conventional improvement are offered as follows:

$$\begin{cases} \bar{G}(1) = X(1) + P_o \cdot \cos\omega \\ \bar{G}(2) = X(2) + P_o \cdot \sin\omega \end{cases} \tag{3.3.3}$$

where ω denotes the angle between the adjusted gravity and the positive direction of X-axis. The position coordinates of the robot in the next step are offered as follows:

$$\begin{cases} X_{j+1}(1) = X_j(1) + l \cdot \cos\varphi \\ X_{j+1}(2) = X_j(2) + l \cdot \sin\varphi \end{cases} \tag{3.3.4}$$

where φ denotes the robot position angle and satisfies the component of the resultant force $F_{sumx} > 0$ on the X-axis, otherwise, if the component $F_{sumx} < 0$ on the X-axis, then we have:

$$\begin{cases} X_{j+1}(1) = X_j(1) - l \cdot \cos\varphi \\ X_{j+1}(2) = X_j(2) - l \cdot \sin\varphi \end{cases} \tag{3.3.5}$$

This paper mainly focuses on studying the path planning under the classical grooved continuous obstacle model. As shown in Figure 5, assuming that the influence radius of obstacle P_o = 1.5, if we adjust the gravitational field gain and the repulsion coefficient κ = 50, β = 5, an artificial potential field prevents the robot from deadlock. In all of the following figures, the small circles represent the obstacle, and the inverted triangle marks the virtual target position. However, the path is disordered inside the concave obstacle obviously, leading to a longer and unsmooth path. In order to improve the quality of the path, we need to adjust the virtual position. Ge and Cui (2000) analyses the causes of jitter and adds an exponential term to the gravitational field function to eliminate the singular value. In addition, a sensitivity parameter is introduced into the repulsive field function to control the distance between the robot and the obstacle in the process of motion. The jitter phenomenon is that the sub-target points are singular points and unstable, which makes the robot swing back and forth between multiple equilibrium points near the sub target points. Fan et al. (2005) uses the method of adding a disturbance to the gravitational field so that the target point is no longer a singular point. Drawing on these methods, we design a newly exponential form sub-target to eliminate singularity of the route sequences. The coordinates of virtual sub-target are province as follows:

$$\begin{cases} G(1) = X(1) + P_o \cdot \cos\omega \cdot e^{\arctan(\pi \cdot |X(1)|)} \cdot \alpha \\ G(2) = X(2) + P_o \cdot \sin\omega \cdot e^{\arctan(\pi \cdot |X(2)|)} \cdot \alpha \end{cases} \tag{3.3.6}$$

3.4 The elimination of path singularity

In this section, we analyse the temporary virtual targets generated by conventional IAPF and exponential form improved methods.

1 Exponential factor coefficient α should meet the following inequality:

$$1 < e^{\arctan(\pi \cdot X(i))} < 1 + \varepsilon \tag{3.4.1}$$

where $0 < \varepsilon < 1$, $i = 1, 2$, since $0 < \alpha < 1$,

$$\frac{1}{\alpha} < e^{\arctan(\pi \cdot X(i))} < \frac{2}{\alpha} \tag{3.4.2}$$

suppose that the robot moves in the first quadrant of the XY-plane, the exponential factor $e^{\arctan(\pi \cdot X(i))}$ is monotonic increasing:

$$\lim_{X(i) \to +\infty} e^{\arctan(\pi \cdot X(i))} = e^{\frac{\pi}{2}} \tag{3.4.3}$$

Figure 5 Conventional IAPF path planning in concave obstacle, (a) motion planning (b) turning angle change (see online version for colours)

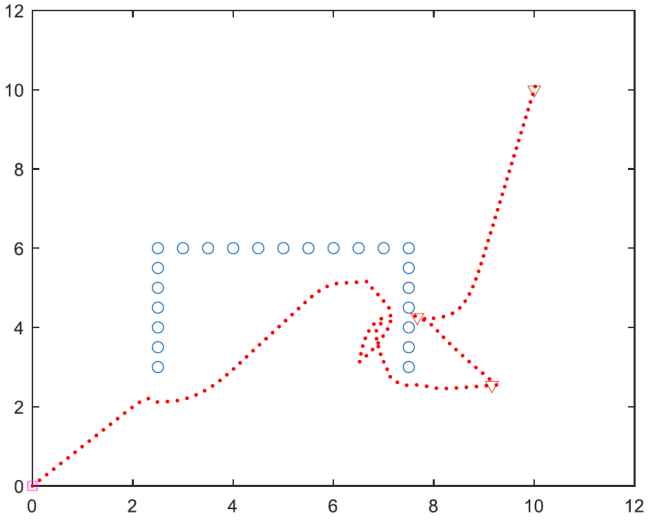

(a)

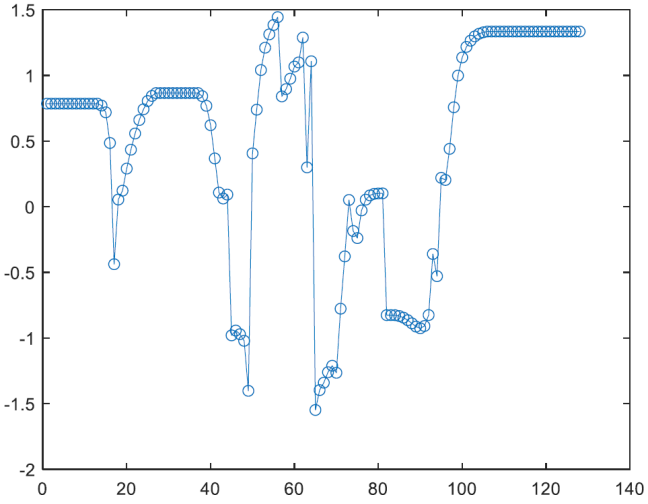

(b)

Figure 6 Proposed method path planning in concave obstacle, (a) motion planning (b) turning angle changes chart (see online version for colours)

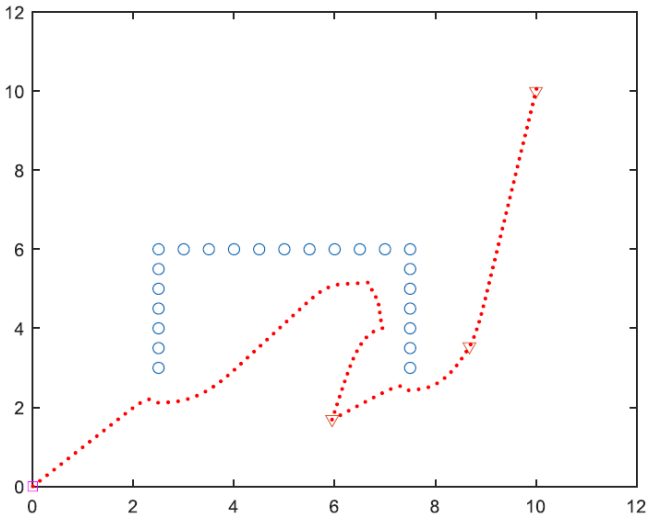

(a)

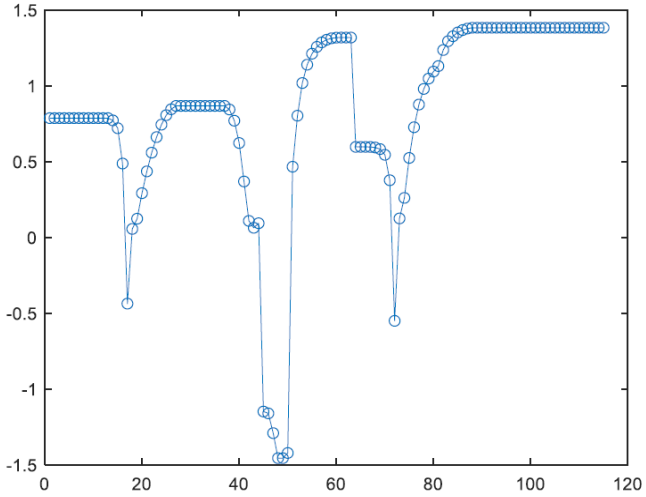

(b)

Inequality (3.4.2) is satisfied only when the value of α is equal or less than 0.3.

2 A robot judges whether it is in the local minimum area according to the conditions (3.1.2) in k^{th} iteration. Assuming that resultant force F_{sum} consists of the gravitational force by virtual target $\bar{G}$ under the conventional improved APF and repulsion force of obstacles, the coordinates of $\bar{G}$ is offered as follows:

$$\begin{cases} \bar{G}(1) = X_k(1) + P_o \cdot \cos\omega \\ \bar{G}(2) = X_k(2) + P_o \cdot \sin\omega \end{cases} \tag{3.4.4}$$

For convenience, we ignore the influence of the repulsion force. The robot position angle in the k^{th} iteration φ^k is expressed as:

$$\begin{aligned} \varphi_k &= \arctan\frac{-\kappa\left\|\bar{G}(2) - X_k(2)\right\|}{-\kappa\left\|\bar{G}(1) - X_k(1)\right\|} \\ &= \arctan\frac{-\kappa P_o \cdot \sin\omega}{-\kappa P_o \cdot \cos\omega} \\ &= \arctan(\tan\omega) \end{aligned} \tag{3.4.5}$$

note that if $\omega \in \left[0, \frac{\pi}{2}\right)$, there exists $\varphi_k = \arctan(\tan\omega)$ $= \omega$, so we just need to consider that $\omega \in \left[0, \frac{\pi}{2}\right)$.

Assuming that during the j^{th} iteration and the subsequent $j + 1^{\text{th}}$ iteration, the path is disordered, resulting in a redundant sequence of path points in the concave region, which takes a long time to adjust and walk out without losing generality, let $j = k + 1$:

$$\begin{cases} X_j(1) = X_k(1) \pm l \cdot \cos\varphi_k = X_k(1) \pm l \cdot \cos\omega \\ X_j(2) = X_k(2) \pm l \cdot \sin\varphi_k = X_k(1) \pm l \cdot \sin\omega \end{cases} \tag{3.4.6}$$

φ_j is offered as follows:

$$\begin{aligned} \varphi_j &= \arctan\frac{-\kappa\left\|\bar{G}(2) - X_j(2)\right\|}{-\kappa\left\|\bar{G}(1) - X_j(1)\right\|} \\ &= \arctan\frac{-\kappa P_o \cdot \sin\omega \pm l \cdot \sin\omega}{-\kappa P_o \cdot \cos\omega \pm l \cdot \cos\omega} \end{aligned} \tag{3.4.7}$$

by function continuity,

$$\lim_{\omega \to \frac{\pi}{2}} -\kappa P_o \cdot \cos\omega \pm l \cdot \cos\omega = 0 \tag{3.4.8}$$

When the numerator and denominator of the robot position angle expression is 0, just like the singularity in the nonlinear control system, it becomes an uncertain value. Next, we prove that these uncertain values will be removed after introducing the exponential factor and maintain path stability. Assuming that the virtual target generated by exponential improved APF denotes G, robot position angle in the k^{th} iteration is offered as follows:

$$\begin{aligned} \varphi_k &= \arctan\frac{-\kappa\left\|G(2) - X_k(2)\right\|}{-\kappa\left\|G(1) - X_k(1)\right\|} \\ &= \arctan\frac{-\kappa P_o \cdot e^{\arctan(\pi \cdot X_k(2))} \cdot \alpha \cdot \sin\omega}{-\kappa P_o \cdot e^{\arctan(\pi \cdot X_k(1))} \cdot \alpha \cdot \cos\omega} \\ &= \arctan\left(e^{\arctan(\pi \cdot X_k(2)) - \pi \cdot X_k(1))} \cdot \tan\omega\right) \end{aligned} \tag{3.4.9}$$

where φ_j can be expressed as below:

$$\begin{aligned} \varphi_j &= \arctan\frac{-\kappa\left\|G(2) - X_j(2)\right\|}{-\kappa\left\|G(1) - X_j(1)\right\|} \\ &= \arctan\frac{\begin{array}{c} -\kappa P_o \cdot \sin\omega \cdot \alpha \cdot e^{\arctan(\pi \cdot X(2))} \\ \pm l \cdot \sin\left(\arctan\left(e^{\arctan(\pi \cdot X_j(2)) - \pi \cdot X_j(1))}\right) \cdot \tan\omega\right) \end{array}}{\begin{array}{c} -\kappa P_o \cdot \cos\omega \cdot \alpha \cdot e^{\arctan(\pi \cdot X(1))} \\ \pm l \cdot \cos\left(\arctan\left(e^{\arctan(\pi \cdot X_j(2)) - \pi \cdot X_j(1))}\right) \cdot \tan\omega\right) \end{array}} \end{aligned} \tag{3.4.10}$$

Figure 7 Comparison two in 2D situations, (a) conventional IAPF path and turning angle change chart (b) modified path and turning angle change (see online version for colours)

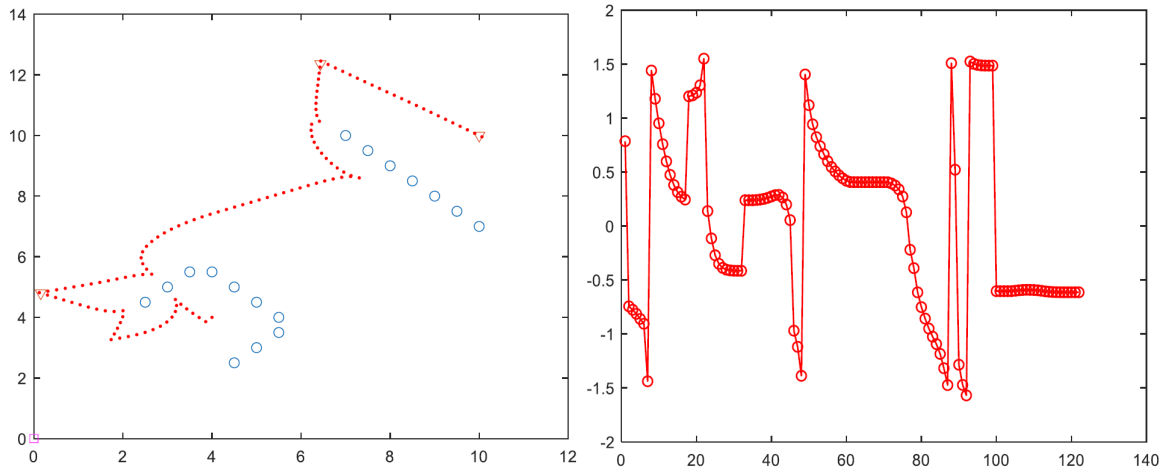

(a)

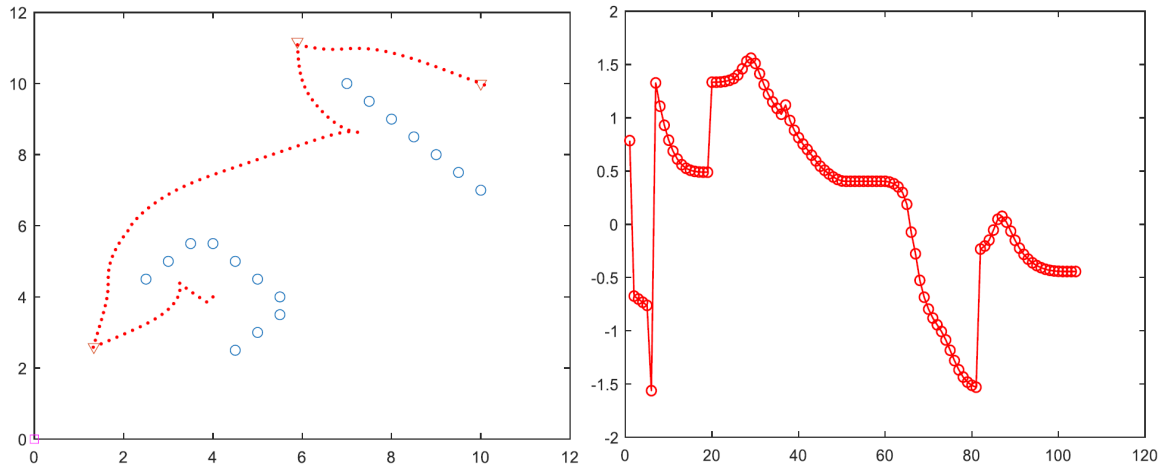

(b)

Since $0 < A = \arctan(e^{\arctan(\pi \cdot X(2)-\pi \cdot X(1))} \cdot \tan\omega) < \frac{\pi}{2}$, if $0<A<1$, there exists $\arctan(A \cdot \tan\omega) < \omega$, suppose that $\arctan(A \cdot \tan\omega) = \omega - \delta$, $\delta \to 0^+$, where δ is a small positive constant, then we have:

$$\begin{aligned} &\lim_{\omega \to \frac{\pi}{2}} \cos\left(\arctan\left(A \cdot \tan_{\omega}\right)\right) = \cos(\omega - \delta) \\ &= \cos\omega \cdot \cos\delta + \sin\omega \cdot \sin\delta = \sin\delta > 0 \end{aligned} \tag{3.4.11}$$

by function continuity,

$$\begin{aligned} &\lim_{\omega \to \frac{\pi}{2}} -\kappa P_o \cdot \cos\omega \cdot \alpha \cdot e^{\arctan(\pi \cdot X(1))} \\ &\pm l \cdot \cos\left(\arctan(A \cdot \tan\omega)\right) = \sin\delta \neq 0 \end{aligned} \tag{3.4.12}$$

$$\begin{aligned} &\lim_{\omega \to \frac{\pi}{2}} -\kappa P_o \cdot \cos\omega \cdot \alpha \cdot e \arctan^{(\pi \cdot X(1))} \\ &\pm l \cdot \sin\left(\arctan(A \cdot \tan\omega)\right) = 0 \end{aligned} \tag{3.4.13}$$

as long as the speed of the numerator approaching zero is greater than the speed of the denominator approaching 0, φ_j can be zero and become a stable angle, which further enhances the path stability.

3.5 *Path evaluation*

We evaluate the advantages and disadvantages of optimisation path from two aspects of timeliness and safety (Zhang and Ming, 2021; Pateloup et al., 2007), security index Q_s is defined as follows:

$$Q = \frac{L}{N+1} \tag{3.5.1}$$

where L denotes the minimum distance from the path to the obstacle, and N is the cumulative number of turning points. The security of a local path is determined by the total number of turning points and the minimum distance. The less the number of turning points, the better the security.

For the above concave obstacle, let other parameters remain unchanged, we use equation (3.1.5) to set virtual targets and take α = 0.3. As shown in Figure 6(a), exponential improved algorithm eliminate redundancy. It can be seen from the comparison of (a) and (b) in

Figures 5(b) and 6(b) that the cumulative number of turns is reduced from 27 to 11, and the minimum distance from robot to obstacle is changed from 0.32 to 0.55. According to equation (3.3.2), security index increases from 0.011 to 0.046. The improved algorithm further reduces redundancy and improves security.

3.6 Simulation experiments

3.6.1 Two-dimensional environment

In order to verify the practicability and effectiveness of our method, the conventional improved APF and the exponential improved APF are simulated by MATLAB. The path planning results and the changes of robot position and angle in typical continuous obstacle spaces such as I-shaped, L-shaped and U-shaped are compared. See Tables 2 and 3 for some main parameter configuration of simulation system.

Table 2 Parameter setting for 2D environment

Parameter	*Value*
Gravitational potential field gain coefficient κ	15
Repulsive potential field gain coefficient β	3
Influence distance of obstacle P_o	2
Step	0.2
Maximum number of loop iterations J	600
Starting position	[4, 4]
Target position	[10, 10]
Exponential coefficient α	0.3

Table 3 Parameter setting for 3D environment

Parameter	*Value*
Gravitational potential field gain coefficient κ	0.04
Repulsive potential field gain coefficient β	0.1
Influence distance of obstacle P_o	30
Step	2
Maximum number of loop iterations J	1,000
Starting position	[10, 10, 0]/[0, 50, 0]
Target position	[180, 120, 20]/ [135, 80, 20]
Exponential coefficient α	0.03

3.6.2 There-dimensional environment

In order to further test the application of robots in production and life, we developed a complex experiment in three-dimensional space. As shown in Figure 8, the obstacle is treated as a group of cylinders. We use a small red circle to mark the starting point, and the green five-pointed star represents the target point.

3.6.3 Simulation analysis

We analyse the safety indicators under the above 2D and 3D environments, the results are shown in Table 4.

In Figure 9(a) and 9(b), the improved algorithm makes the robot reach the target successfully in the above two cases, and the motion trajectory relatively utilised our strategy is smoother. It could be seen from Figure 9(c) that the agent encounters the local minima and fails to goal reachable when there is no modification on model if we move one of a cylinder near to target, while Figure 9(d) shows the good performance of our algorism which is capable of keeping on searching and arriving at goal. Figures 9(e) and 9(f) represent the parameter changes (initial state and goal state). From Table 4, we can see that the path seems to be longer, but it is farther away from obstacles compared with the route in Figure 9(e) which walks around the surface, and meets the requirement of safety standards for robotics. From Table 4, we have observed an average search time of 24.5s during the experimental study while the existing IAPF needs an average search time of 60.5s, resulting in a 59.50%-time savings.

Figure 8 Obstacles distribution map, (a) 3D (b) XY-plane (see online version for colours)

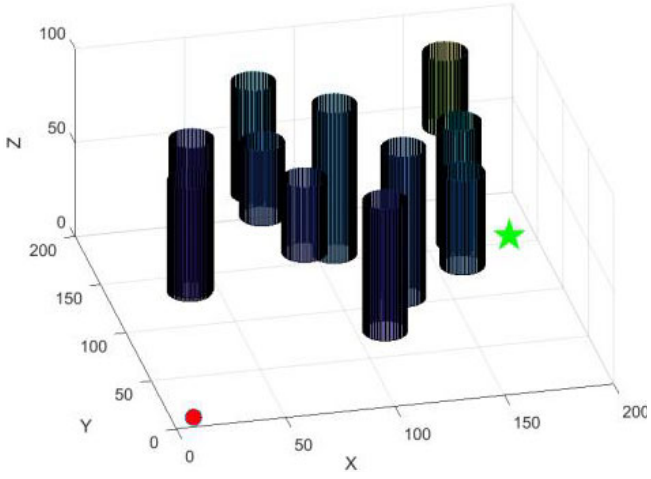

(a)

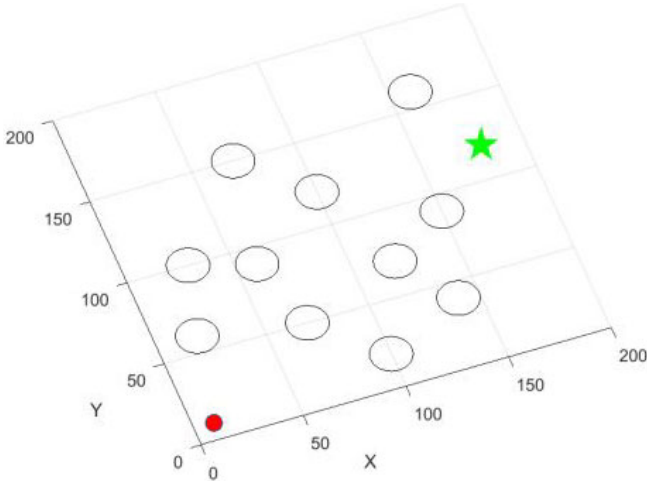

(b)

Figure 9 Comparisons of the two strategies in 3D situations (see online version for colours)

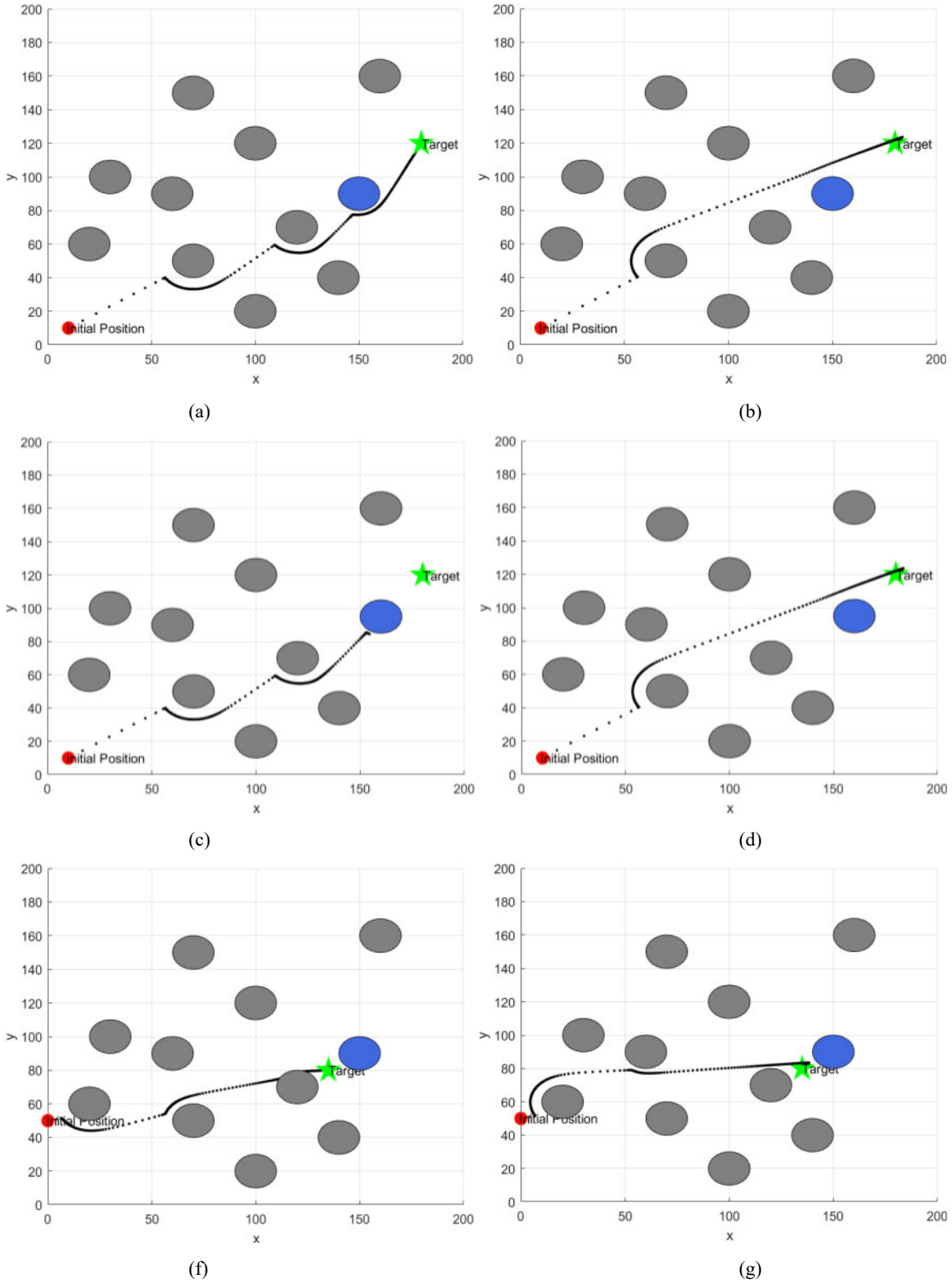

Notes: Left: conventional IAPF and right: our method.

4 Limitations of the research

In this section, we explain some constraints of the proposed technique:

1 The proposed exponential feedback-feedforward MFAC strategy is implemented on a small time-varying and structurally time-varying nonlinear discrete system. The performance of the control law needs to be evaluated for large scale programs to verification for real industrial production.

2 We considered the security that a robot can escape from the dead zone, and the generated waypoints are regularly ordered in order to eliminate unnecessary path backtracking, however, although the improved virtual sub-target position reduces the number of turning angles, smoothness should be thoroughly considered, especially avoidance of the small turning angles.

Table 4 Comparison of two strategies

	Length/m	*Elapsed time/s*	*Minimum distance/m*
2D			
Traditional IAPF	24.2000	0.1200	0.4472
Our method	20.6000	0.0805	0.6708
3D-1			
Traditional IAPF	227.5821	70.50	2.3087
Our method	226.4040	23.50	6.4560
3D-2			
Traditional IAPF	172.1156	80.50	
Our method	235.7566	22.50	6.1717
3D-3			
Traditional IAPF	141.6329	30.50	0.0008
Our method	314.1782	27.50	2.0025

5 Conclusions and future work

In conclusion, based on the research background of auto mobile robot trajectory planning in complex environmental space, to solve the core automobile robotic technologies, this paper focuses on the two major sections of motion planning and trajectory tracking, firstly, a parametric exponential feedback-feedforward control law is constructed according to the existing ICL-MFAC system. Secondly, the optimisation method introduces an exponential form virtual target as a new reference to improve the APF algorithm. By analysing the simulation experiments results, it can be known that the improved algorithm proposed in this paper effectively makes up for the shortcomings of traditional algorithms in path planning under some various complex and harsh conditions and high-precision trajectory tracking. In the future, we will validate the proposed method on practical applications. The future work can be deeply studied from the aspects of road scenarios recognition by image processing (Wu et al., 2020) and human-robot interaction dynamic model (Shi et al., 2021), so as to improve the robustness of the controller.

Nowadays, mobile robots are widely used in medical, education, family and other fields, in order to meet service needs and shorten application time, we improve robot performance and prolong service life. We explore the best path planning scheme, which is of great significance for the wide application of mobile robots. Compared with the traditional trajectory tracking control and path planning algorithms, we have made the following innovations: A parametric exponential feedback feedforward control law is constructed according to ICL-MFAC system; virtual target method with exponential term is used to plan the path. Mobile robot can find a short and smooth path.

References

Eduardo, J.M., Angel, L. and Manuel, O. (2019) 'Dynamic window based approaches for avoiding obstacles in moving', *Robotics and Autonomous Systems*, Vol. 118, pp.112–130.

Fan, X., Li, S. and Chen, T. (2005) 'Robot dynamic obstacle avoidance planning based on new artificial potential field function', *Control Theory & Application*, Vol. 22, No. 5, pp.703–707.

Ge, S.S. and Cui, Y.J. (2000) 'New potential functions for mobile robot path planning', *IEEE Trans on Robotic and Automation*, Vol. 16, No. 5, pp.615–620.

Jinchao, G. and Yu, G. (2013) 'Path planning of mobile robot based on improved potential field', *Information Technology Journal*, Vol. 12, No. 11, pp.2188–2194.

Luo, Q.Y., Zhang, H., Wang, H. and Xie, X.Z. (2011) 'Application of improved artificial potential field approach in local path planning for mobile robot', *Computer Engineering and Design*, Vol. 32, No. 4, pp.1411–1413.

Mateo, L.A. and Sugimoto, K. (2015) 'Two-degree-of-freedom control with tuning of both prefilter and feedforward controller', *International Journal of Advanced Mechatronic Systems*, Vol. 6, No. 6, pp.277–288.

Naik, K.J., Pedagandam, M. and Mishra, A. (2021) 'Workflow scheduling optimisation for distributed environment using artificial neural networks and reinforcement learning', *International Journal of Computational Science and Engineering*, Vol. 24, No. 6, pp.653–670.

Noueili, L., Chagra, W. and Ksouri, M.L. (2017) 'Optimal iterative learning control for a class of non-minimum phase systems', *International Journal of Modelling, Identification and Control*, Vol. 28, No. 3, pp.284–294.

Pateloup, V., Chanal, H., Duc, E. and Ray, P. (2007) 'HSM pocketing tool path evaluation proposition of performance criteria', *International Journal of Machining and Machinability of Materials*, Vol. 2, No. 2, pp.206–221.

Patra, A.K. and Mohapatra, S.K. (2022) 'Coordinated control of PI type PSS and MISO PI type SSSC-based damping controller design using improved grasshopper optimisation algorithm', *International Journal of Computational Science and Engineering*, Vol. 25, No. 4, pp.421–436.

Ren, Y. and Hou, Z. (2020) 'Robust model-free adaptive iterative learning formation for unknown heterogeneous non-linear multi-agent systems', *IET Control Theory & Applications*, Vol. 14, No. 4, pp.654–663.

Shi, D., Zhang, W., Zhang, W., Ju, L. and Ding, X. (2021) 'Human-centred adaptive control of lower limb rehabilitation robot based on human-robot interaction dynamic model', *Mechanism and Machine Theory*, Vol. 162, pp.1–16, Art. No. 104340.

Shin, Y. and Kim, E. (2021) 'Hybrid path planning using positioning risk and artificial potential fields', *Aerospace Science and Technology*, Vol. 112, pp.1–13, Art. No. 106640.

Song, R., Liu, Y.C. and Bucknall, R. (2019) 'Smoothed A* algorithm for practical unmanned surface vehicle path planning', *Applied Ocean Research*, Vol. 83, pp.9–20.

Wu, H., Li, Y., Zhang, J. and Kuang, Y. (2020) 'Fast road scenarios recognition of intelligent vehicles by image processing', *International Journal of Information and Communication Technology*, Vol. 18, No. 1, pp.1–15.

Wu, Y. and Liu, G-P. (2019) 'Networked multi pipeline pressure synchronous coordinated predictive control based on the model free adaptive method', *International Journal of Engineering Systems Modelling and Simulation*, Vol. 11, No. 2, pp.60–68.

Xueqiang, D. (2014) 'Path planning of mobile robot based on modified artificial potential field method', *Journal of Shandong University of Technology (Natural Science Edition)*, Vol. 28, No. 1, pp.38–41.

Zhang, S. and Ming, Z. (2021) 'Research on improved artificial potential field local path planning based on active security', *Journal of Zhengzhou University (Engineering Science)*, Vol. 42, No. 5, pp.32–36.

Zhao, D. and Li, W. (2017) 'Robot path planning based on improved artificial potential field', *Machinery Design & Manufacture*, Vol. 7, No. 317, pp.252–255.